nature chemistry

Article

https://doi.org/10.1038/s41557-023-01207-z

A high-dimensional microfluidic approach for selection of aptamers with programmable binding affinities

Received: 4 August 2022

Accepted: 17 April 2023

Published online: 5 June 2023

Check for updates

Dingran Chang[1,12], Zongjie Wang[2,12], Connor D. Flynn[3,4], Alam Mahmud[5], Mahmoud Labib[1,4,6], Hansen Wang[1], Armin Geraili[1], Xiangling Li[1], Jiaqi Zhang[1], Edward H. Sargent[4,5,7,8] & Shana O. Kelley[1,2,3,4,8,9,10,11]

Aptamers are being applied as affinity reagents in analytical applications owing to their high stability, compact size and amenability to chemical modification. Generating aptamers with different binding affinities is desirable, but systematic evolution of ligands by exponential enrichment (SELEX), the standard for aptamer generation, is unable to quantitatively produce aptamers with desired binding affinities and requires multiple rounds of selection to eliminate false-positive hits. Here we introduce Pro-SELEX, an approach for the rapid discovery of aptamers with precisely defined binding affinities that combines efficient particle display, high-performance microfluidic sorting and high-content bioinformatics. Using the Pro-SELEX workflow, we were able to investigate the binding performance of individual aptamer candidates under different selective pressures in a single round of selection. Using human myeloperoxidase as a target, we demonstrate that aptamers with dissociation constants spanning a 20-fold range of affinities can be identified within one round of Pro-SELEX.

Precise control over the binding affinities between biomolecules is one of the critical means by which nature allows thousands of types of biomolecule to operate in tandem with molecular-level control in heavily crowded environments. Moreover, molecules with well-defined binding affinities for a specific target—thus called affinity reagents—are essential for many applications, including biosensing, diagnostics, imaging and therapeutics. For example, the binding affinity between a target analyte and its specific biorecognition element is the determinative factor that defines the dynamic range of a biosensor[1,2]. High-affinity recognition molecules with low dissociation constants (K_d) are sought for point-of-care applications to enable rapid binding events and low limits of detection. On the other hand, low-affinity reagents with fast association and dissociation rates have been used in real-time monitoring applications[3–5], because they can resolve the dynamic changes in their target analyte level. The advancement of detection modalities with extremely high resolution and low background levels has also made it possible for low-affinity binding reagents to achieve high detection sensitivity[2,6,7]. Hence, to meet the diverse requirements of different sensing scenarios, it is highly desirable to be able to generate recognition molecules with desired binding affinities against a specific target.

[1]Leslie Dan Faculty of Pharmacy, University of Toronto, Toronto, Ontario, Canada. [2]Department of Biomedical Engineering, McCormick School of Engineering, Northwestern University, Evanston, IL, USA. [3]Department of Chemistry, University of Toronto, Toronto, Ontario, Canada. [4]Department of Chemistry, Weinberg College of Arts & Sciences, Northwestern University, Evanston, IL, USA. [5]Department of Electrical and Computer Engineering, University of Toronto, Toronto, Ontario, Canada. [6]Peninsula Medical School, Faculty of Health, University of Plymouth, Plymouth, UK. [7]Department of Electrical and Computer Engineering, McCormick School of Engineering, Northwestern University, Evanston, IL, USA. [8]International Institute for Nanotechnology, Northwestern University, Evanston, IL, USA. [9]Department of Biochemistry, Feinberg School of Medicine, Northwestern University, Chicago, IL, USA. [10]Simpson Querrey Institute, Northwestern University, Chicago, IL, USA. [11]Chan Zuckerberg Biohub Chicago, Chicago, IL, USA. [12]These authors contributed equally: Dingran Chang, Zongjie Wang. e-mail: shana.kelley@northwestern.edu

https://doi.org/10.1038/s41557-023-01207-z

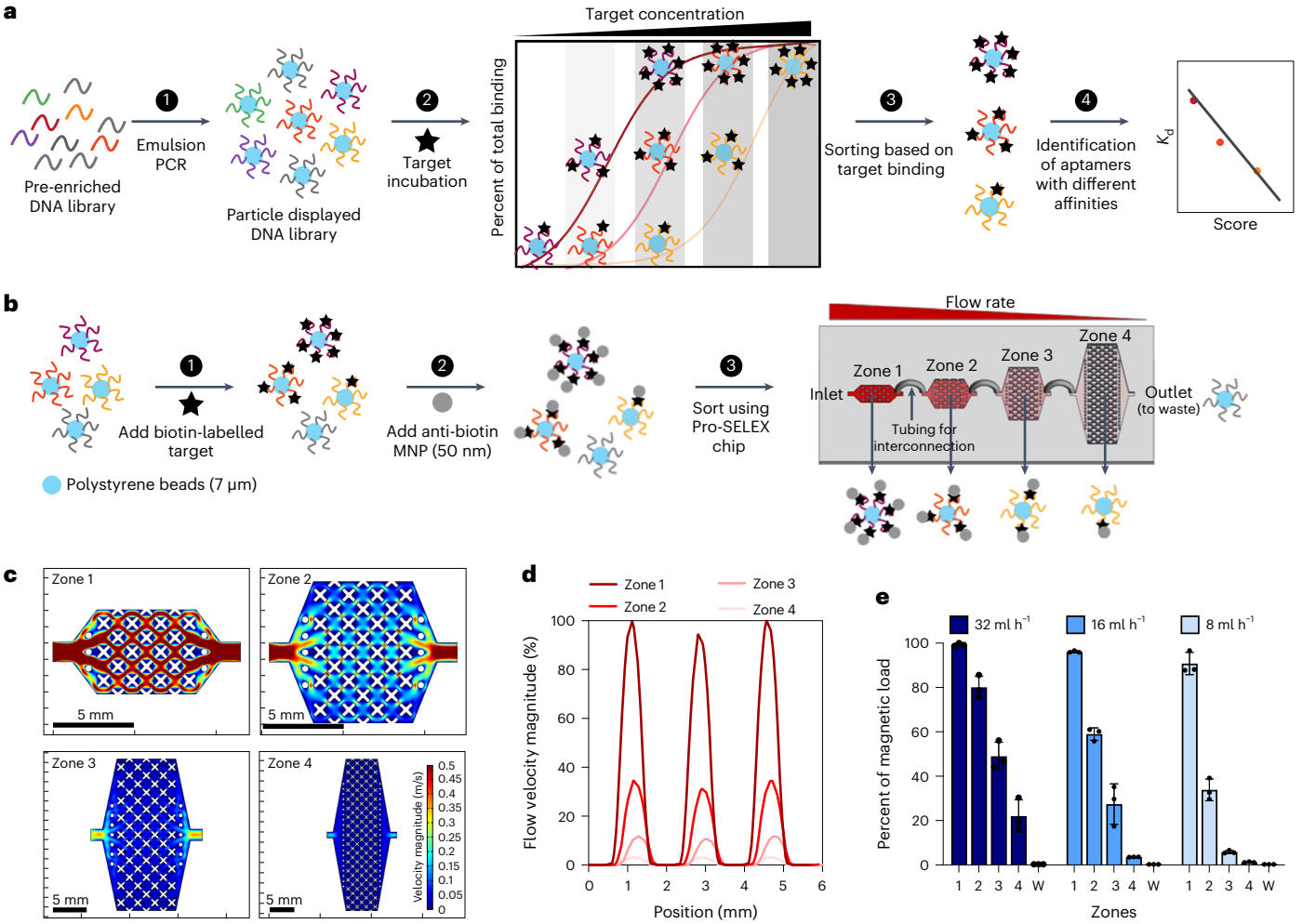

Fig. 1 | Quantitative isolation of aptamers with different binding affinities via a high-dimensional microfluidic approach. a, Overall workflow. Shaded bands represent the target concentration (darker colour indicates higher concentration). **b**, Isolation of aptamer particles with different levels of target binding using Pro-SELEX chips. **c**, Separation rationale: simulated linear flow velocity profile. The formation of capture pockets was observed in the valley of X-shaped microstructures. **d**, Magnitude of linear flow velocity. **e**, Determination of the median magnetic load of particles captured by Pro-SELEX at different flow rates (8, 16 and 32 ml h^{-1}). Data are presented as mean values, and the error bars represent the standard deviation of three replicates. W represents particles collected from the outlet (waste).

Nucleic-acid aptamers have garnered substantial interest as versatile affinity reagents and as promising alternatives to antibodies over the past three decades[8–10]. In recent years, aptamers have demonstrated great potential in real-time monitoring and wearable sensing applications[11–15]. Compared to antibodies, aptamers offer several unique features, including high stability, compact size, cost-effective mass synthesis, minimal batch-to-batch variation, non-immunogenic properties and amenability to site-specific chemical modification[8,16,17]. Despite these attractive features, the use of aptamers in biosensing is relatively limited. One reason for this is a lack of high-quality aptamers for many biomolecular targets[16]. Conventional procedures for aptamer selection through SELEX are labour-intensive, time-consuming and incapable of producing aptamers with programmable binding affinities. A typical SELEX experiment requires 10 to 15 rounds of selection to allow the target-binding sequences to dominate the nucleic acid pool[16,18,19]. This inefficiency is due to the inability of traditional SELEX to separate aptamer candidates with diverse binding affinities in each round, as well as the introduction of undesired biases—such as polymerase chain reaction (PCR) bias and amplification of parasitic sequences—through repeated rounds of selection. These factors also make the binding affinities of the selected aptamers unpredictable, requiring a number of sequences to be tested to identify an aptamer with desired properties.

Recent advancements in SELEX technologies with improved sequence partitioning efficiency, such as CE-SELEX[20], Non-SELEX[21], M-SELEX[22] and particle display selection technology[23], have provided solutions for the aptamer-selection challenge. However, none of these methods are able to quantitatively generate aptamers with defined binding affinities. Here we describe a new approach, referred to as Pro-SELEX, for quantitative isolation of aptamers with programmable binding affinities. Our workflow consists of particle display, magnetic particle sorting, high-dimensional and parallelized selection and high-content bioinformatics. Using this workflow, we are able to profile the binding performance of individual aptamer candidates at different target concentrations in a single round of selection. As a proof of concept, we selected aptamers specific to human myeloperoxidase (MPO), an emerging diagnostic and prognostic biomarker of coronary artery disease[24,25]. We successfully isolated a number of anti-MPO aptamers with pre-defined binding affinities (K_d) and developed algorithms relating selection data to this important biological parameter.

Results

The overall Pro-SELEX approach is summarized in Fig. 1. Aptamer libraries displayed on particles are incubated with the binding target, where they are expected to bind to differing numbers of analyte molecules based on affinity. Magnetic nanoparticles are used to label the aptamer particles (APs) according to number of analyte molecules bound, and the aptamer particles are then sorted into different compartments of a microfluidic chip based on magnetic content. Pools of aptamers are generated based on the material collected in each compartment and sequenced. Comparative bioinformatics are employed to analyse the representation of individual aptamers and confirm the validity of sequences as true-positive hits as well as infer relative affinity ranges.

Development of Pro-SELEX selection platform

To measure the relative affinity of each aptamer sequence in a nucleic acid library, particle display techniques[23] can be used to transform individual aptamer candidates from a solution-based aptamer library into monoclonal APs via emulsion PCR, where each particle presents many copies of a single nucleic-acid sequence on its surface (Fig. 1a). The AP libraries can then be incubated with a specific target over a range of concentrations. Based on the Langmuir isotherm, the target binding level of an AP is dependent on the target concentration and the binding affinity of the aptamer coated on its surface, where half of the aptamer molecules will be bound to the target when the target concentration is equal to the K_d of the aptamer. APs with different binding levels can then be separated and collected using a high-resolution microfluidic sorting approach followed by sequencing analysis to identify aptamers with different binding affinities based on their binding performance at different target concentrations.

To accurately partition APs with different levels of target binding, we developed a magnetic labelling and microfluidic sorting approach (Fig. 1b). Polystyrene particles (7 µm in diameter) were used to prepare APs. After incubation of the APs with a biotinylated target of interest, the particles were labelled with anti-biotin magnetic nanoparticles (MNPs, 50 nm in diameter) to convert the target binding into a magnetic content. The labelled mixture was then sorted and isolated using a microfluidic device (Pro-SELEX chip). This device features four capture zones with differing linear velocities to allow differential sorting of APs with varying levels of magnetic content. Owing to the low magnetic susceptibility of MNPs, each capture zone contains microfabricated structures to create localized regions of low flow velocity and enhanced capture dynamics (Supplementary Fig. 1). The first zone exhibits the highest linear velocity and thus retains APs with high magnetic content, as the retaining magnetic force overcomes the drag force exerted by the high flow velocity. The ensuing three zones exhibit gradually reduced linear velocities (Fig. 1d; for simulation information see Fig. 1c). This design allows APs to be separated and captured in different zones according to their target binding levels. We demonstrated that the Pro-SELEX chip is able to sort the particles based on their magnetic content (Fig. 1e and Supplementary Fig. 2). It is worth noting that the stringency and resolution of magnetic separation of the Pro-SELEX chip are programmable by adjusting the chip flow rate (Fig. 1e). Similar device design has been used to perform profiling of cellular proteins and nucleic acids as well as rare cell capture, demonstrating superior throughput and recovery rate compared to fluorescence-activated cell sorting (FACS) and magnetic-activated cell sorting (MACS)[26–29]. We now demonstrate the utility of this type of device for aptamer selection.

Validation of the sorting performance of the Pro-SELEX chip

In the first suite of experiments, we used thrombin aptamers as a test case to validate the approach (Fig. 2a). We first tested whether the Pro-SELEX chip could sort APs with different levels of target binding. Particles coated with thrombin-03 aptamer[23] (03-particles) with varying target binding levels were prepared by incubating the particles with a range of thrombin concentrations, from 1 pM to 1 nM, followed by labelling with MNPs (Fig. 2b). These 03-particles were then sorted using Pro-SELEX chips at flow rates of 8 ml h^{-1} and 16 ml h^{-1}, and distinctive sorting profiles were generated (Fig. 2c,d). The particles with high magnetic content (1 nM and 100 pM) were primarily captured in zone 1 of the chip at a flow rate of 8 ml h^{-1} and partially shifted to zone 2 upon increasing the flow rate to 16 ml h^{-1}, whereas particles with lower magnetic content were mainly collected in later zones and almost all of the non-target bound particles were detected in the waste. This observation indicates that the Pro-SELEX chip is able to sort and capture APs based on their target binding levels, employing several flow rates to stratify the sorting profile.

Next, we explored whether the Pro-SELEX approach could separate APs with different binding affinities. Two types of AP were prepared carrying comparable copy numbers of either thrombin-03 (K_d = 7.04 pM) or thrombin-TBA (K_d = 2.6 nM)[23,30] (Supplementary Fig. 3). Both APs, together with primer-coated particles, were tested with three thrombin concentrations and analysed using flow cytometry (Fig. 2e–g) and the Pro-SELEX chip (Fig. 2h–j). When using a thrombin concentration of 1 µM, which is substantially higher than the K_d of both aptamers, both APs became saturated by the target and were captured in zone 1 of the chip. When the target concentration dropped to 1 nM, a substantial separation was observed such that the high-affinity 03-particles remained in zone 1 and the low-affinity TBA-particles were binned in zones 2 and 3. When the target concentration further decreased to 1 pM, most TBA-particles were collected in the waste, whereas a substantial fraction of the 03-particles were still captured in the chip. Notably, less than 0.5% of the primer-coated particles were captured by the chip at a flow rate of 8 ml h^{-1}, regardless of the thrombin concentrations, showcasing the high capture specificity of the Pro-SELEX chip. We further investigated the effect of flow rate on the nonspecific capture of aptamers to ensure that nonbinders can efficiently be removed during the selection process (Supplementary Fig. 4). Together, these results demonstrated that the Pro-SELEX chip is capable of separating APs with distinctive binding affinities, where target concentrations play a prominent role in determining the separation efficiency.

Selection of MPO aptamers using Pro-SELEX

We next explored whether we could use the Pro-SELEX platform to efficiently generate aptamers. We selected MPO as the model target for testing the capability of Pro-SELEX for aptamer selection. An initial random DNA library containing ~1×10^{14} random DNA molecules was first subjected to a pre-enrichment step consisting of three rounds of both counter selections against undesired targets and conventional SELEX towards MPO immobilized beads to remove nonspecific binders and reduce the sequence space of the library (Supplementary Table 1 and Supplementary Fig. 5). The enriched library was then used as a template to prepare AP libraries through emulsion PCR (Supplementary Fig. 6). The AP libraries were tested at five MPO concentrations (10 pM, 100 pM, 1 nM, 10 nM and 100 nM), in an attempt to isolate aptamers with K_d within this range. It was critical to ensure that the MPO molecules were available in excess and not depleted during the target incubation, especially when testing low target concentrations, to confirm that the binding between APs and MPO follows the Langmuir isotherm (Supplementary Table 2). The AP libraries were then sorted by Pro-SELEX chips at two flow rates, 16 ml h^{-1} and 32 ml h^{-1} (Fig. 3a). It required less than 20 min for the Pro-SELEX chip to sort 5×10^7 APs, which is faster than the FACS-based sorting method[23]. Particles captured by each zone within the ten chips were then collected (Fig. 3b,c). As expected, we clearly observed that the fractions of APs captured by Pro-SELEX chips decreased upon lowering the target concentration, and the sorting profiles of the AP libraries were shifted when using a faster flow rate, highlighting the high resolution of our approach.

The particles collected from zones 1–3 of each chip, together with the unsorted aptamer population, for a total of 31 DNA pools,

https://doi.org/10.1038/s41557-023-01207-z

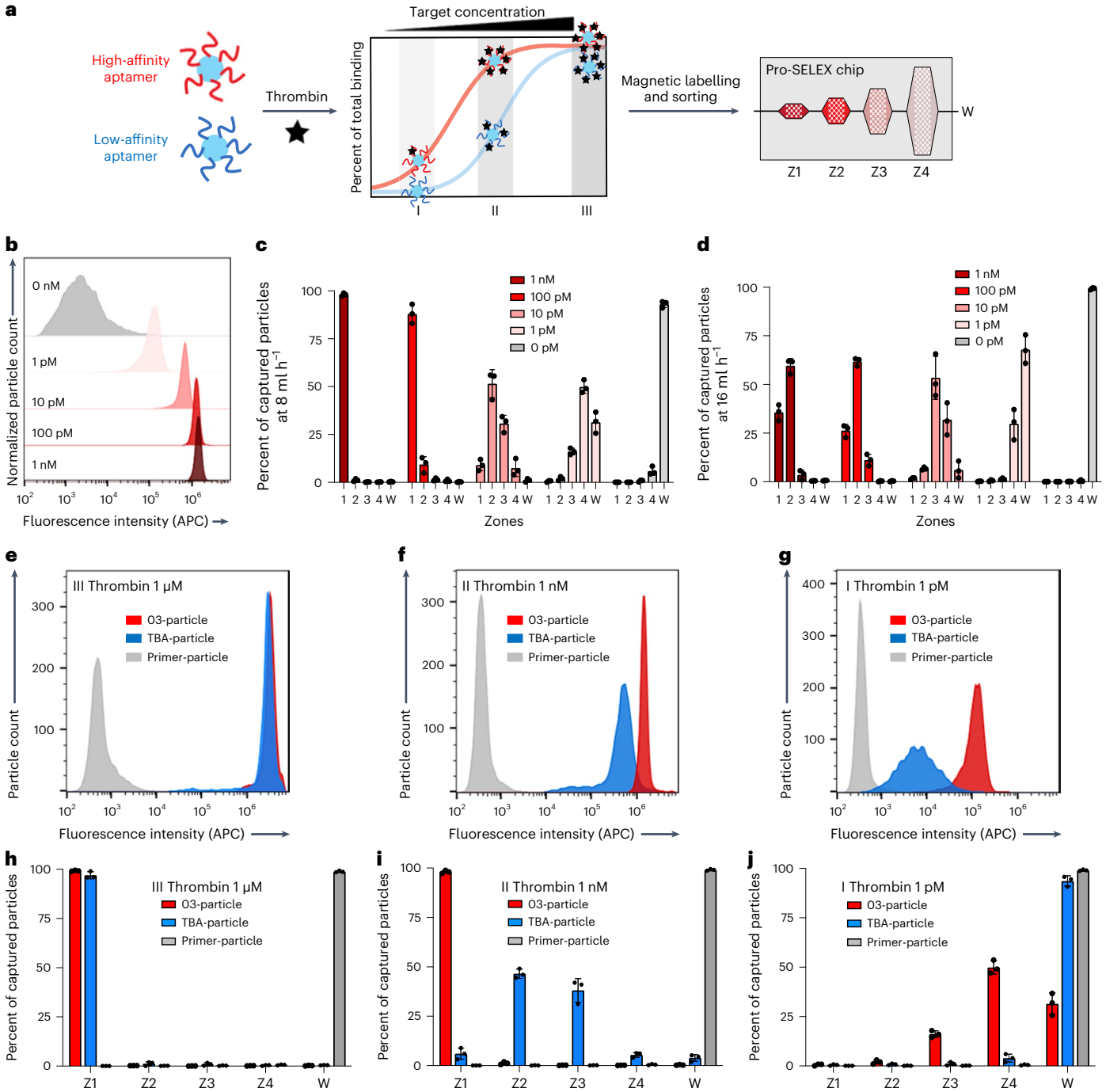

Fig. 2 | Validation of the sorting performance of the Pro-SELEX chip using anti-thrombin aptamers with different binding affinities. a, Workflow of the validation experiments. Z1–Z4, zones 1–4; W, waste. Shaded bands represent the target concentration (darker colour indicates higher concentration). **b**, Evaluation of the binding performance of thrombin-03-coated APs at thrombin concentrations of 1 nM, 100 pM, 10 pM, 1 pM and 0 pM. The particles are labelled with MNPs and anti-MNPs labelling check reagent-APC and analysed by flow cytometry. **c**,**d**, Determination of the capture profile of particle-displayed thrombin-03 aptamer prepared using different thrombin concentrations at flow rates of 8 ml h^{-1} (**c**) and 16 ml h^{-1} (**d**). Data are presented as mean values, and the error bars represent the standard deviation of three replicates. **e**–**g**, Analysis of particle-displayed thrombin aptamer 03, TBA and a primer sequence after incubation with 1 μM (**e**), 1 nM (**f**) and 1 pM (**g**) thrombin molecules. The particles are labelled with MNPs and anti-MNPs labelling check reagent-APC and analysed by flow cytometry. **h**–**j**, Sorting of the particle-displayed thrombin aptamers 03, TBA and a primer sequence using Pro-SELEX chip at a flow rate of 8 ml h^{-1} with 1 μM (**h**), 1 nM (**i**) and 1 pM (**j**) thrombin molecules. Data are presented as mean values, and the error bars represent the standard deviation of three replicates.

were subjected to high-throughput sequencing (HTS). We also created a scoring tool, AptaZ, which was employed to comprehensively analyse the fold of enrichment of each aptamer candidate from 30 DNA pools and generate a *Z* score (details are provided in Supplementary Discussion and Fig. 3d). Aptamer candidates that can survive multiple target concentrations, especially low concentrations at two flow rates, and be repeatedly captured by the chips would generate high *Z* scores (Fig. 3e). Eight MPO-aptamer candidates, MPO-01 to MPO-08, with diverse *Z* scores, were randomly chosen for characterization (Supplementary Table 3). All eight aptamers demonstrated an

https://doi.org/10.1038/s41557-023-01207-z

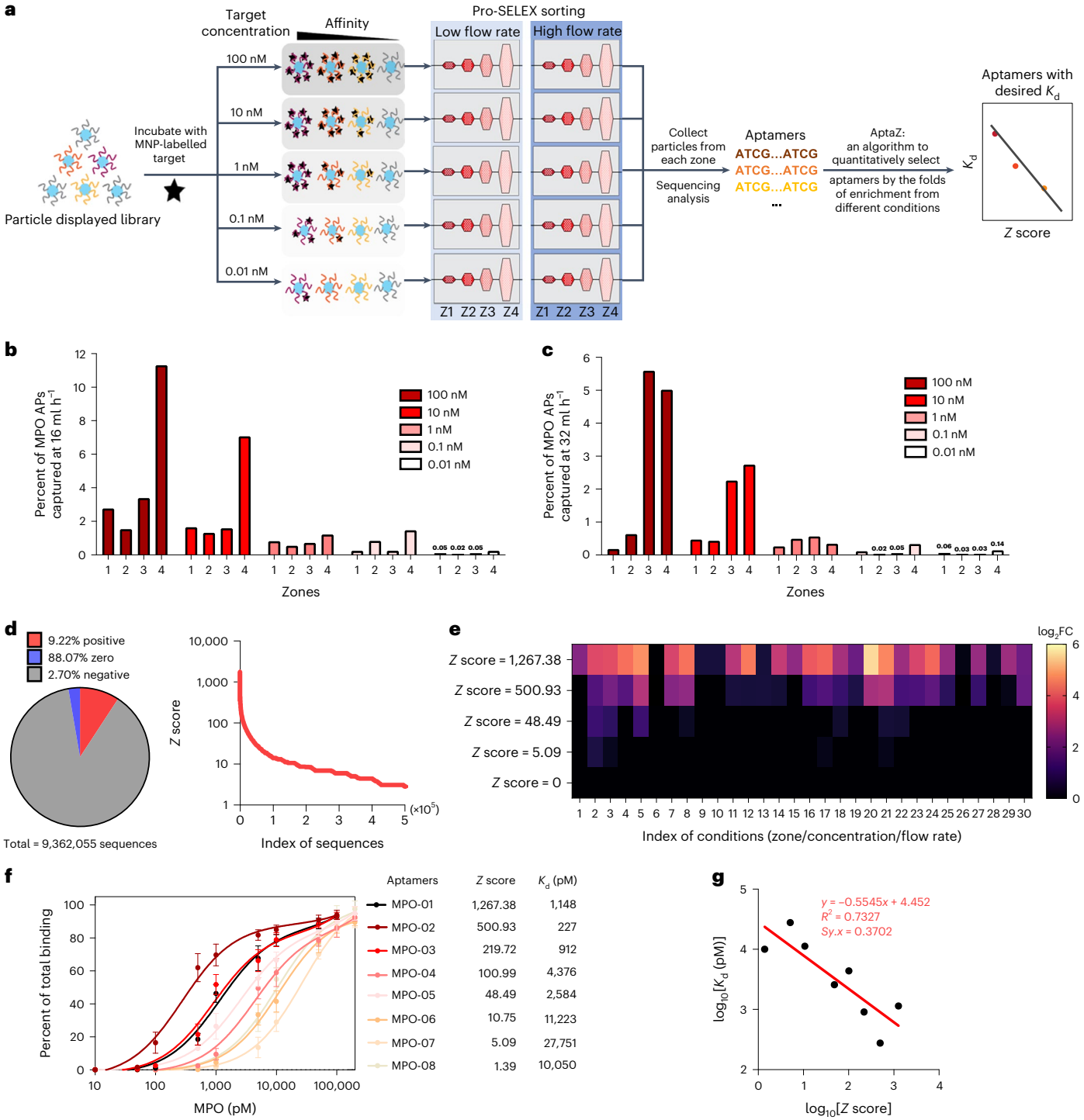

Fig. 3 | Isolation of anti-MPO aptamers with different binding affinities via a high-dimensional microfluidic-based approach. a, Workflow of the selection experiments. Five MPO concentrations (100 nM, 10 nM, 1 nM, 100 pM and 10 pM) were tested at flow rates of 16 and 32 ml h^{-1} for the screening experiments. Particles were collected from individual capture zones (Z1–Z3) and analysed by high-throughput sequencing and the AptaZ tool for aptamer identification. **b**,**c**, APs collected from zones 1–4 of the Pro-SELEX chips at flow rates of 16 ml h^{-1} (**b**) and 32 ml h^{-1} (**c**). **d**, Distribution of calculated *Z* score over the pool of sequences presented in MPO selection. **e**, Heatmap of fold enrichment in all 30 conditions of sequences with different *Z* scores. The AptaZ algorithm comprehensively considers the fold enrichment from different conditions to generate *Z* scores to quantitatively rank the aptamers. FC, fold change. **f**, Eight candidates with different *Z* scores were expressed on particles and incubated with Cy5-labelled MPO before analysis via flow cytometry. Each line represents a fitted Langmuir isotherm. Data are presented as mean values, and error bars represent the standard deviation of three replicates. **g**, The relationship between calculated *Z* score and validated K_d derived from the eight candidates. The *Z* score correlates with the K_d value in a linear fashion according to curve fitting.

affinity for MPO with K_d values ranging from 227 pM to 27.8 nM (Fig. 3f and Supplementary Fig. 7). A linear relationship was observed between the K_d values of the eight candidates and their calculated *Z* scores based on curve fitting (Fig. 3g), indicating the potential of using *Z* scores to search for the aptamer candidates with desired binding affinities.

https://doi.org/10.1038/s41557-023-01207-z

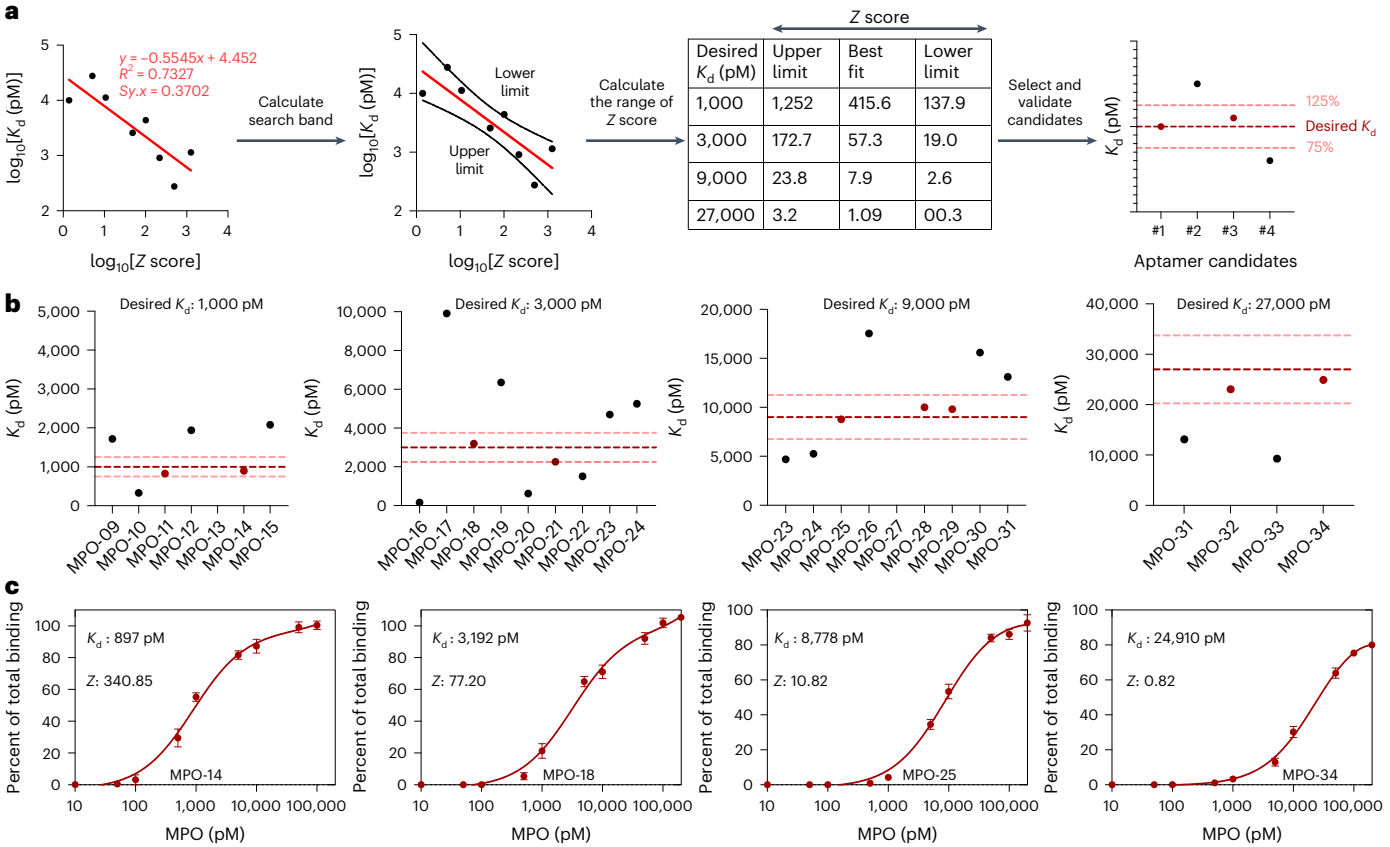

Fig. 4 | Quantitative isolation of anti-MPO aptamers with desired affinities based on their *Z* score. a, Strategy for validation. A K_d search band was generated based on the K_d–*Z* score curve fit. The *Z*-score ranges of four desired values of K_d (1,000 pM, 3,000 pM, 9,000 pM and 27,000 pM) were calculated. Several aptamer candidates within the *Z*-score ranges could be tested and the difference between their actual K_d and the desired K_d then calculated to evaluate the accuracy of *Z*-score-based aptamer identification. **b**, Evaluation of the accuracy of using *Z* scores to identify MPO aptamers with K_d values of 1,000 pM, 3,000 pM, 9,000 pM and 27,000 pM. Red dots represent the aptamers with an actual K_d with <25% difference from the desired K_d. The data points for MPO-13 (K_d = 9,580 pM) and APO-27 (K_d = 27,700 pM) are outside the axis limits and are not shown. **c**, The binding curve of the best-fit aptamer candidates. Polystyrene particles coated with aptamers MPO-14, MPO-18, MPO-25 or MPO-34 were incubated with Cy-5-labelled MPO before analysis via flow cytometry. The red line represents the results of fitting a Langmuir binding isotherm to the MPO binding data. Error bars represent the standard deviation of three replicates, and the centres of the error bars represent mean values.

Quantitative selection of MPO aptamers with desired affinities

We next explored whether the *Z* score could be used to quantitatively screen aptamers with desired binding affinities. A search band was generated based on the correlation between the *Z* score and the K_d values of the validated MPO aptamers (Fig. 4a). We set the desired K_d values as 1,000 pM, 3,000 pM, 9,000 pM and 27,000 pM and calculated their theoretical *Z* score ranges based on the search band. Aptamer candidates within this range were then chosen and examined for their binding affinities, and the differences between their experimental K_d and the desired K_d were calculated. We defined a difference smaller than 25% as a 'great fit'.

By evaluating the binding affinity of multiple MPO-aptamer candidates in different *Z*-score ranges (Supplementary Fig. 8 and Supplementary Table 4), we found that the success rate in identifying a 'great fit' was between 20% and 50%, suggesting that by testing no more than five aptamer candidates within the *Z*-score range, we can identify one aptamer with the desired binding affinity (Fig. 4b). The 'best fits' for the requested affinities are MPO-14 with a K_d of 897 pM, MPO-18 with a K_d of 3,192 pM, MPO-25 with a K_d of 8,778 pM and MPO-34 with a K_d of 24,910 pM (Fig. 4c; their secondary structures are provided in Supplementary Fig. 9). The K_d values of the tested aptamers spanned more than 100-fold. The selected aptamers also demonstrated excellent specificities for MPO (Supplementary Fig. 10) as well as the potential to be used to analyse biological samples (Supplementary Fig. 11). MPO-16 revealed the highest binding affinity (K_d = 166 pM); its sequence, secondary structure, binding specificity and binding performance in biological samples are highlighted in Supplementary Fig. 12. It should be noted that the normal MPO level from a healthy middle-aged population has been reported to be <640 pM, with higher MPO levels being associated with increased risk of cardiovascular diseases[31]. We believe that the anti-MPO aptamers with different binding affinities reported here will become valuable tools in future MPO monitoring applications.

Discussion

We developed an aptamer-generation method, Pro-SELEX, which enables efficient and quantitative generation of aptamers with desired binding affinities. Unlike conventional SELEX methods, which rely on iterative rounds of selection to screen for aptamer candidates (Fig. 5a), our approach monitors the binding performance of individual aptamer candidates at different target concentrations in a single round of selection (Fig. 5b), taking advantage of the high level of parallelization enabled by high-dimensional microfluidics. Current iterations of SELEX, such as CE-SELEX and particle display, despite their substantially improved efficiency in generating aptamers, still select for aptamers with the highest affinities (Fig. 5c). Unfortunately, high-affinity aptamers might not be suitable for all applications. For example, affinity

https://doi.org/10.1038/s41557-023-01207-z

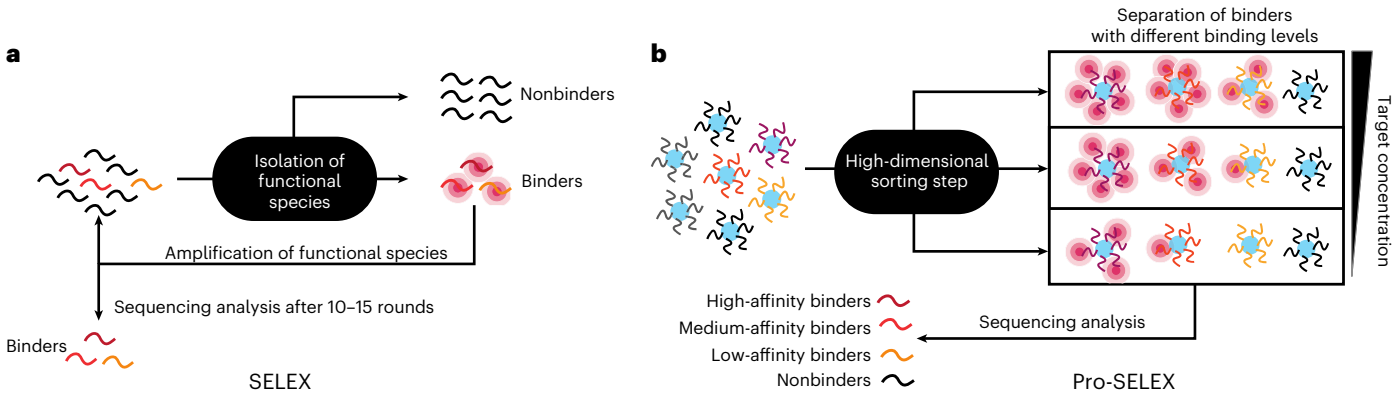

c

Aptamer selection technologies	Pro-SELEX	SELEX[16,18,19]	Particle display[23]	CE-SELEX[20]
Rounds required	1 (3 pre-enrichment rounds)	10–15	3–5 (3 pre-enrichment rounds)	1–5
Programmable affinity?	K_d is programmable within dynamic testing range	Not programmable	K_d is programmable, but only for high-affinity aptamers	Not programmable
Throughput	High (multiple conditions in one round)	Low (1 condition in each round)	Low (1 condition in each round)	Low (1 condition in each round)

Fig. 5 | Comparison of Pro-SELEX with current aptamer-selection technologies. a, Conventional SELEX strategy. **b**, Pro-SELEX strategy. **c**, A table summarizing the performance criteria of Pro-SELEX versus current aptamer-selection technologies.

receptors with suitable K_d should be selected based on the target concentration range to achieve quantitative biomolecular recognition, as the dynamic range of single-site binding typically spans 81-fold changes in target concentrations, which is dependent on the K_d of the receptors[2]. If the K_d of a receptor is substantially lower than the relevant concentration range, the resulting saturated signal will not change over the detection range[2]. A strategy to manipulate the dynamic range of sensing is to combine receptors with different target affinities[1,32]. This naturally raises the need to generate aptamers with different K_d. In addition, lower-affinity receptors with fast binding kinetics (high on rate and off rate) are ideal for continuous monitoring as they allow for rapid equilibration with the surrounding target[4,33]. The development in recent years of sophisticated detection modalities with considerably lower levels of background and digital outputs makes it possible to quantify molecules in log dynamic ranges at concentrations much lower than the K_d (refs. 34–36). By exploiting these types of sensing mechanism, low-affinity receptors can also achieve high detection sensitivity. Collectively, it will be advantageous to have the capability of generating receptors with customizable binding affinities to meet the requirements of diverse applications. The Pro-SELEX platform was developed to fulfil this need.

The Pro-SELEX approach is also highly programmable and can be easily customized to suit various other applications. For example, the particle size used in this platform is large enough (diameter of 7 µm) to capture a wide range of targets, from small molecules to viruses or bacteria. Given the high efficiency of Pro-SELEX and the broad applications of aptamers during the SARS-CoV-2 pandemic[37–39], our platform can be applied for the rapid generation of antivirus aptamers during the early stage of a pandemic. The time required for Pro-SELEX and SELEX to complete is summarized in Supplementary Table 5. In addition, recent advances in incorporating non-natural nucleotides with diverse structures and functional groups into aptamers would lead to aptamers with enhanced binding performance and expanded target range[40–43]. We believe our approach can be adapted to accommodate these unnatural nucleotides to efficiently produce modified aptamers.

Online content

Any methods, additional references, Nature Portfolio reporting summaries, source data, extended data, supplementary information, acknowledgements, peer review information; details of author contributions and competing interests; and statements of data and code availability are available at https://doi.org/10.1038/s41557-023-01207-z.

References

1. Drabovich, A. P. et al. Smart aptamers facilitate multi-probe affinity analysis of proteins with ultra-wide dynamic range of measured concentrations. *J. Am. Chem. Soc.* **129**, 7260–7261 (2007).
2. Wilson, B. D. et al. Re-evaluating the conventional wisdom about binding assays. *Trends Biochem. Sci.* **45**, 639–649 (2020).
3. Arroyo-Currás, N. et al. Real-time measurement of small molecules directly in awake, ambulatory animals. *Proc. Natl Acad. Sci. USA* **114**, 645–650 (2017).
4. Fercher, C. et al. Recombinant antibody engineering enables reversible binding for continuous protein biosensing. *ACS Sens.* **6**, 764–776 (2021).
5. Plaxco, K. W. et al. Seconds-resolved, in situ measurements of plasma phenylalanine disposition kinetics in living rats. *Anal. Chem.* **93**, 4023–4032 (2021).
6. Xue, L. et al. Solid-state nanopore sensors. *Nat. Rev. Mater.* **5**, 931–951 (2020).
7. Sevenler, D. et al. Beating the reaction limits of biosensor sensitivity with dynamic tracking of single binding events. *Proc. Natl Acad. Sci. USA* **116**, 4129–4134 (2019).

8. Wang, T. et al. Three decades of nucleic acid aptamer technologies: lessons learned, progress and opportunities on aptamer development. *Biotechnol. Adv.* **37**, 28–50 (2019).
9. Liu, J. et al. Functional nucleic acid sensors. *Chem. Rev.* **109**, 1948–1998 (2009).
10. Song, S. et al. Aptamer-based biosensors. *Trends Anal. Chem.* **27**, 108–117 (2008).
11. Wang, B. et al. Wearable aptamer-field-effect transistor sensing system for noninvasive cortisol monitoring. *Sci. Adv.* **8**, eabk0967 (2022).
12. Nakatsuka, N. et al. Aptamer-field-effect transistors overcome Debye length limitations for small-molecule sensing. *Science* **362**, 319–324 (2018).
13. Mage, P. L. et al. Closed-loop control of circulating drug levels in live animals. *Nat. Biomed. Eng.* **1**, 0070 (2017).
14. Ferguson, B. S. et al. Real-time, aptamer-based tracking of circulating therapeutic agents in living animals. *Sci. Transl. Med.* **5**, 213ra165 (2013).
15. Zhao, C. et al. Implantable aptamer-field-effect transistor neuroprobes for in vivo neurotransmitter monitoring. *Sci. Adv.* **7**, eabj7422 (2021).
16. Qian, S. et al. Aptamers from random sequence space: accomplishments, gaps and future considerations. *Anal. Chim. Acta* **1196**, 339511 (2022).
17. Li, F. et al. Aptamers facilitating amplified detection of biomolecules. *Anal. Chem.* **87**, 274–292 (2015).
18. Ellington, A. D. et al. In vitro selection of RNA molecules that bind specific ligands. *Nature* **346**, 818–822 (1990).
19. Tuerk, C. et al. Systematic evolution of ligands by exponential enrichment: RNA ligands to bacteriophage T4 DNA polymerase. *Science* **249**, 505–510 (1990).
20. Mendonsa, S. D. et al. In vitro evolution of functional DNA using capillary electrophoresis. *J. Am. Chem. Soc.* **126**, 20–21 (2004).
21. Berezovski, M. et al. Non-SELEX selection of aptamers. *J. Am. Chem. Soc.* **128**, 1410–1411 (2006).
22. Lou, X. et al. Micromagnetic selection of aptamers in microfluidic channels. *Proc. Natl Acad. Sci. USA* **106**, 2989–2994 (2009).
23. Wang, J. et al. Particle display: a quantitative screening method for generating high-affinity aptamers. *Angew. Chem. Int. Ed.* **53**, 4796–4801 (2014).
24. Zhang, R. et al. Association between myeloperoxidase levels and risk of coronary artery disease. *JAMA* **286**, 2136–2142 (2001).
25. Baldus, S. et al. Myeloperoxidase serum levels predict risk in patients with acute coronary syndromes. *Circulation* **108**, 1440–1445 (2003).
26. Labib, M. et al. Single-cell mRNA cytometry via sequence-specific nanoparticle clustering and trapping. *Nat. Chem.* **10**, 489–495 (2018).
27. Labib, M. et al. Tracking the expression of therapeutic protein targets in rare cells by antibody-mediated nanoparticle labelling and magnetic sorting. *Nat. Biomed. Eng.* **5**, 41–52 (2021).
28. Wang, Z. et al. Efficient recovery of potent tumour-infiltrating lymphocytes through quantitative immunomagnetic cell sorting. *Nat. Biomed. Eng.* **6**, 108–117 (2022).
29. Wang, Z. et al. Ultrasensitive detection and depletion of rare leukemic B cells in T cell populations via immunomagnetic cell ranking. *Anal. Chem.* **93**, 2327–2335 (2021).
30. Bock, L. C. et al. Selection of single-stranded DNA molecules that bind and inhibit human thrombin. *Nature* **355**, 564–566 (1992).
31. Tang, W. H. W. et al. Usefulness of myeloperoxidase levels in healthy elderly subjects to predict risk of developing heart failure. *Am. J. Cardiol.* **103**, 1269–1274 (2009).
32. Vallée-Bélisle, A. et al. Engineering biosensors with extended, narrowed or arbitrarily edited dynamic range. *J. Am. Chem. Soc.* **134**, 2876–2879 (2012).
33. Tu, J. et al. The era of digital health: a review of portable and wearable affinity biosensors. *Adv. Funct. Mater.* **30**, 1906713 (2020).
34. Deng, R. et al. Recognition-enhanced metastably shielded aptamer for digital quantification of small molecules. *Anal. Chem.* **90**, 14347–14354 (2018).
35. Das, J. et al. Reagentless biomolecular analysis using a molecular pendulum. *Nat. Chem.* **13**, 428–434 (2021).
36. Wang, L. et al. Rapid and ultrasensitive electromechanical detection of ions, biomolecules and SARS-CoV-2 RNA in unamplified samples. *Nat. Biomed. Eng.* **6**, 276–285 (2022).
37. Zhang, Z. et al. High-affinity dimeric aptamers enable the rapid electrochemical detection of wild-type and B.1.1.7 SARS-CoV-2 in unprocessed saliva. *Angew. Chem. Int. Ed.* **60**, 24266–24274 (2021).
38. Li, J. et al. Diverse high-affinity DNA aptamers for wild-type and B.1.1.7 SARS-CoV-2 spike proteins from a pre-structured DNA library. *Nucleic Acids Res.* **49**, 7267–7279 (2021).
39. Yang, G. et al. Identification of SARS-CoV-2-against aptamer with high neutralization activity by blocking the RBD domain of spike protein 1. *Signal Transduct. Target. Ther.* **6**, 227 (2021).
40. Lapa, S. A. et al. The toolbox for modified aptamers. *Mol. Biotechnol.* **58**, 79–92 (2016).
41. Gawande, B. N. et al. Selection of DNA aptamers with two modified bases. *Proc. Natl Acad. Sci. USA* **114**, 2898–2903 (2017).
42. Gordon, C. K. L. et al. Click-particle display for base-modified aptamer discovery. *ACS Chem. Biol.* **14**, 2652–2662 (2019).
43. Pfeiffer, F. et al. Identification and characterization of nucleobase-modified aptamers by click-SELEX. *Nat. Protoc.* **13**, 1153–1180 (2018).

Methods

Materials

Carboxyl polystyrene particles (7 µm, #PC06004) were purchased from Bangs Laboratories. Dulbecco's phosphate-buffered saline (DPBS; #14190250), streptavidin (Cy5, #SA1011), Dynal MyOne C1 streptavidin Dynabeads (65001), biotinylated peroxidase (#432040), a PureLink Quick gel extraction kit (K210012), an EZ-Link Micro NHS-PEG4-biotinylation kit (#21955) and dNTP Mix (#R0192) were ordered from Thermo Fisher Scientific. Light mineral oil (#M5310), 2-butanol (#294810), *N*-(3-dimethylaminopropyl)-*N*′-ethylcarbodiimide hydrochloride (EDC, #161462), *N*-hydroxysuccinimide (NHS, #130672), human serum (H4522-100ML) and imidazole hydrochloride (#13386) were purchased from Sigma Aldrich. Anti-biotin microbeads ultrapure (#130-105-637) and labelling check reagents-APC (#130-122-219) were purchased from Miltenyi Biotech. Recombinant human MPO (3174-MP-250) was ordered from R&D Systems. Lambda exonuclease (#M0262S) was ordered from New England Biolabs (NEB). GoTaq G2 Hot Start Taq Polymerase (#M7405) was purchased from Promega. ABIL® EM 90 was obtained from Evonik. Recombinant human BNP protein (#ab87200) and recombinant human RANTES protein (#ab269212) were ordered from Abcam. Biotinylated thrombin (#69723) was obtained from Fisher Scientific. DT-20-M Gamma tubes were ordered from IKA Works. Water was purified with a Millipore Milli-Q Biocel water purification system.

All DNA oligonucleotides (Supplementary Table 1) were obtained from Integrated DNA Technologies and purified by 10% denaturing (8 M urea) polyacrylamide gel electrophoresis, and their concentrations were determined using a NanoDrop spectrophotometer. The library was 90-nt long, consisting of a 50-nt variable region flanked by two 20-nt primer sites (5′-AGCAGCACAGAGGTCAGATG-N50-AAGTGTAGTGTCTCCGTGGC-3′). The forward primer sequence was 5′-AGCAGCACAGAGGTCAGATG-3′ and the reverse primer was 5′-GCCACGGAGACACTACACTT-3′. The sequencing adaptors were 5′-ACACTCTTTCCCTACACGACGCTCTTCCGATCT-NNNN-AGCAGCACAGAGGTCAGATG-3′ for the forward-primer adaptor and 5′-GTGACTGGAGTTCAGACGTGTGCTCTTCCGATCTGCC ACGGAGACACTACACTT-3′ for the reverse-primer adaptor.

Chip fabrication and operation

The microfluidic device was fabricated using a protocol combining three-dimensional (3D) printing and soft lithography techniques, as described in ref. 44. In brief, the master mould was manufactured by a stereolithographic 3D printer (Microfluidics Edition 3D Printer, Creative CADworks) using the 'CCW master mould for PDMS' resin (Resinworks 3D) with a layer thickness of 50 µm. The actual chips were fabricated by casting polydimethylsiloxane (Sylgard 184, Dow Chemical) on the printed moulds, followed by 120-min incubation at 70 °C for curing. Cured polydimethylsiloxane replicas were peeled off, punched and plasma-bonded to no. 1 glass thickness coverslips (260462, Ted Pella) to finish the chip. Before use, the chips were conditioned with a binding buffer (DPBS with 2.5 mM $MgCl_2$, 1 mM $CaCl_2$ and 0.01% TWEEN-20) to remove air bubbles. During operation, each chip was attached to arrayed N52 NdFeB magnets (D14-N52, K&J Magnetics) and fluidically connected to a digital syringe pump (Fusion 100, Chemyx) under the withdrawn mode.

Finite-element simulation

Numerical simulation of the flow velocity pattern within the microfluidic device was carried out using COMSOL Multiphysics (version 5.6, COMSOL) using the 3D creeping flow module. The key parameters for the simulation were as follows: boundary condition—pressure of 0 Pa with suppression of backflow; wall condition—no slip; mesh size—physics-controlled, fine.

Scanning electron microscopy

The fabricated chips were coated with 15-nm Au using a desktop sputter coater (Denton Desk II, Leica). The coated chips were imaged under a field-emission scanning electron microscope (SU5000, Hitachi) using 5-kV accelerating voltage and high-vacuum mode.

Preparation of biotin-labelled protein targets

MPO protein, as well as the proteins used for counter selection, including human serum proteins, BNP and RANTES, were biotinylated using an EZ-Link Micro NHS-PEG4-biotinylation kit (Thermo Fisher Scientific). The free biotin was removed by a Zeba Desalt spin column with 7-K molecular-weight cutoff (10 ml, Thermo Fisher Scientific). We measured the biotinylated MPO protein concentration based on absorbance at 280 nm using a NanoDrop spectrophotometer.

Pre-enrichment by SELEX

The DNA library (6×10^{14} random DNA molecules) was diluted with 1 ml of binding buffer and heated at 90 °C for 1 min, followed by annealing at room temperature (r.t.) for 10 min. Magnetic beads (Dynabeads MyOne streptavidin C1, Thermo Fisher Scientific) conjugated with human serum proteins, thrombin, BNP and RANTES were washed twice with binding buffer, and incubated with the DNA library at r.t. for 2 h. The DNA in the supernatant was collected, mixed with MPO (R&D Systems)-conjugated magnetic beads, and incubated at r.t. for 1 h. The beads were washed five times with 500 µl of binding buffer. The MPO-bound DNA molecules were then eluted by adding 100 µl of water and heating at 95 °C for 15 min. The eluted DNA was PCR-amplified and used for the following round of enrichment and AP synthesis. Three rounds of pre-enrichment were performed to remove both nonspecific DNA molecules that bind to other protein targets and inactive DNA molecules that do not bind to MPO protein.

Preparation of forward primer particles

A 1-ml volume of 7-µm carboxyl polystyrene particles (Bangs Laboratories) was washed once with 1 ml of 0.01 N NaOH and three times with 1 ml of nuclease-free water, then resuspended in a 500-µl reaction mixture containing 200 mM NaCl, 0.2 mM 5′-amino-modified FP (or amino-modified thrombin aptamers), 1 mM imidazole chloride, 50% v/v dimethyl sulfoxide and 250 mM EDC (Sigma Aldrich). The free carboxyls on the particles were then converted into amino-reactive NHS ester in the presence of 250 mM EDC and 100 mM NHS in 2-(*N*-morpholino) ethanesulfonic acid (MES) buffer (100 mM, pH 4.7; Thermo Scientific) for 30 min at r.t. The particles were then conjugated with 20 mM amino-PEG12 (Thermo Scientific) in MES buffer for 1 h. The particles were washed three times with 1 ml of TE (10 mM Tris, pH 8.0, 0.1 mM EDTA), suspended in 1 ml of TE buffer and stored at 4 °C.

Preparation of aptamer particles

Emulsion PCR. The oil phase (prepared freshly each time) was composed of 3% ABIL® EM90 and 0.05% Triton X-100 in mineral oil. The aqueous phase consisted of 1× GoTaq PCR buffer (Promega), 25 mM $MgCl_2$, 3.5 mM of each dNTP (Thermo Fisher Scientific), 3 µM 5′ phosphorylated reverse primer (Phos-RP), 0.5 U μl^{-1} of GoTaq Hot Start Polymerase (Promega), 2 pM template DNA and 5×10^7 forward-primer-coated particles in a total volume of 1 ml. Water-in-oil emulsions were prepared by adding 1 ml of the aqueous phase to 7 ml of the oil phase in a DT-20 tube (IKA) locked into the Ultra-Turrax device (IKA). This addition was performed dropwise over 30 s while the mixture was stirred at 650 r.p.m. in the Ultra-Turrax. After adding the aqueous phase, we continued stirring the mixture for 5 min. The emulsions were distributed in 100-µl aliquots into ~80 wells of a 96-well PCR plate. We performed PCR under the following cycling conditions: 94 °C for 3 min, followed by 50 cycles of 94 °C for 15 s, 58 °C for 30 s and 72 °C for 60 s.

Emulsion PCR clean-up. After PCR, each PCR well was mixed with 50 µl of 2-butanol to break the emulsion. The broken emulsions were then transferred to a 50-ml tube. Next, 150 µl of 2-butanol were added to each PCR well to collect the leftover emulsions, then transferred to

the 50-ml collection tube. After vortexing for 30 s, the particles were pelleted by centrifugation at 2,500*g* for 5 min. After carefully removing the oil phase, we resuspended the particles in 1 ml of emulsion breaking buffer (100 mM NaCl, 1% Triton X-100, 10 mM Tris-HCl, pH 7.5 and 1 mM EDTA) and transferred them to a new 1.5-ml tube. After vortexing for 30 s and centrifugation for 90 s at 15,000*g*, we removed the supernatant. Particles were then washed three times with TE buffer by centrifugation followed by resuspension in 500 µl of TE.

Single-strand generation. To generate single-stranded DNA, we first removed the supernatant by centrifugation. We then treated the particles with 100 U of Lambda exonuclease (NEB) in 500 µl of reaction buffer (67 mM glycine-KOH (pH 9.4), 2.5 mM $MgCl_2$, 0.01% (vol/vol) Triton X-100) at 37 °C for 1 h, followed by inactivation of the reaction by heating at 80 °C for 15 min. The particles were then washed three times with 1 ml of TE buffer, suspended in 1 ml of TE buffer and stored at 4 °C.

AP quality control

Forward primer conjugation. To test the conjugation efficiency of the forward primers, we incubated 1 µM Cy5-labelled FP complementary sequence (Cy5-FP′) with 1 µl of forward-primer particles in 100 µl of binding buffer at 60 °C for 10 min, then cooled them at r.t. for 10 min. The particles were washed twice with 100 µl of binding buffer and analysed with a Cytoflex flow cytometer (Beckman Coulter Life Science). Acquired data were analysed using FlowJo software (version 10.8.1, FlowJo).

AP monoclonality. Based on the Poisson distribution, most particles would be monoclonal when <35% of the particles contain PCR products[23]. To confirm this, we annealed the APs with Cy5-labelled reverse primer in binding buffer at 60 °C for 10 min then cooled them at r.t. for 10 min. The particles were then washed twice with 100 µl binding buffer and analysed by flow cytometry.

Determining the aptamer copy number on each AP. Quantitative PCR was performed with a CFX384 Real-Time PCR detection system (Bio-Rad) to estimate the aptamer copy number for each AP. Calibration samples were prepared by adding 6×10, 6×10^2, 6×10^3, 6×10^4, 6×10^5, 6×10^6, 6×10^7, 6×10^8 or 6×10^9 templates into a 10-µl reaction containing 250 nM each of forward and reverse primer, ~8,000 forward-primer-coated particles, 5 µl of GoTaq PCR Master Mix (Promega) and 0.5× SYBR green (Life Technologies). Test samples were prepared identically, but with ~10,000 APs. From the threshold cycle, we quantified ~6×10^8 sequences on 10,000 APs. Because only ~20% of APs displayed template sequences, the average copy number of sequences on each template-bearing AP was ~3×10^5.

Pro-SELEX screening

During Pro-SELEX screening, we incubated 5×10^7 aptamer particles with biotin-labelled MPO protein at different concentrations (see Supplementary Table 2 for detailed experimental conditions) in selection buffer (DPBS with 2.5 mM $MgCl_2$, 1 mM $CaCl_2$, 0.01% TWEEN-20, 0.2% BSA). To ensure the MPO molecules are not depleted during selection, the reaction volumes were increased when using lower concentrations of the target. After 1 h of incubation, the beads were washed three times with selection buffer. We then magnetically labelled the aptamer particle-captured MPO proteins by incubating the particles with 20 µl of anti-biotin microbeads (Miltenyi Biotech) in 1 ml of selection buffer for 15 min at r.t. The particles were then washed with binding buffer twice and sorted by Pro-SELEX microfluidic devices. The APs captured at each capture zone of the Pro-SELEX microfluidic devices were collected and stored at 4 °C.

High-throughput sequencing

For each collected aptamer pool and the unsorted DNA pool, two rounds of PCR were performed to add adaptor sequences and sequencing indexes. The amplified sequences were then purified using agarose gel electrophoresis and a PureLink Quick gel extraction kit, quantified using a NanoDrop spectrophotometer, and sent to McMaster Genomics Facility for sequencing on an Illumina MiSeq.

Bioinformatics

Raw sequencing data were processed using the Illumina Basespace online platform to sort tagged sequence pools and output sequence data in FASTQ format. Paired-end reads were merged using USEARCH (v10)[45] and the primers were then trimmed using Cutadapt (V3.5)[46]. Sequences containing less than perfect complementarity were discarded to minimize sequencing errors in the dataset. FASTA format trimmed sequences were dereplicated and tagged with the copy number using USEARCH. Read counts were then generated in the format of tab-delimited text files. The files were processed by the AptaZ script written in MATLAB (version 2021a, MathWorks) to calculate the corresponding *Z* score for each sequence. Calculated *Z* scores were exported as CSV files for visualization and validation. The source code of AptaZ can be accessed, free of charge, at https://github.com/dwangnu/AptaZ.

Affinity measurement

After sequencing analysis, we performed particle PCR to synthesize APs displaying each unique aptamer candidate sequence. Each particle PCR reaction (100 µl) consisted of 1× GoTaq PCR Master Mix (Promega), 25 mM $MgCl_2$, 2 µM phos-RP, 10 nM aptamer template and 5×10^6 FP-coated particles. PCR was carried out under the following cycling conditions: 94 °C for 3 min, followed by 30 cycles of 94 °C for 15 s, 58 °C for 30 s and 72 °C for 30 s. To avoid particle aggregation and increase particle PCR efficiency, we vortexed the reaction every four cycles after the 94 °C denaturing step. We then removed the reverse strands using Lambda exonuclease as described above. We then incubated 1 µl of the APs with Cy5-RP and measured the AP fluorescence intensity using flow cytometry to test for particle PCR efficiency. For affinity measurement, different concentrations of biotinylated MPO (10 pM to 200 nM) were incubated with a fixed amount of the APs (2×10^4 particles) in selection buffer for 1 h at room temperature. The unbound MPO was washed away with selection buffer, after which streptavidin-labelled Cy5 was introduced and incubated for 15 min to label the bound MPO. The particles were washed with binding buffer, and median fluorescence intensities were quantified via flow cytometry and FlowJo software (version 10.8.1, FlowJo).

Reporting summary

Further information on research design is available in the Nature Portfolio Reporting Summary linked to this article.

Data availability

The main data supporting the results in this study are available within the paper and its Supplementary Information . The sequencing data files are too large to be publicly shared, but they are available from the corresponding author upon reasonable request. The chip design (in the format of STL) and running protocol of the microfluidic chip will be available free of charge from the publisher's website as a supplementary file. Source data are provided with this paper.

Code availability

The code corresponding to the AptaZ algorithm can be accessed at https://github.com/dwangnu/AptaZ.

References

44. Wang, Z. et al. Ultrasensitive and rapid quantification of rare tumorigenic stem cells in hPSC-derived cardiomyocyte populations. *Sci. Adv.* **6**, eaay7629 (2020).
45. Edgar, R. C. & Bateman, A. Search and clustering orders of magnitude faster than BLAST. *Bioinformatics* **26**, 2460–2461 (2010).

46. Martin, M. Cutadapt removes adapter sequences from high-throughput sequencing reads. *EMBnet J.* **17**, 10–12 (2011).

Acknowledgements

This research was supported in part by the Canadian Institutes of Health Research (grant no. FDN-148415) and the Collaborative Health Research Projects Program (CIHR/NSERC partnered). This research is part of the University of Toronto's Medicine by Design initiative, which receives funding from the Canada First Research Excellence Fund. This research was supported in part by the McCormick Catalyst Fund at Northwestern University.

Author contributions

D.C., Z.W. and S.O.K. conceived and designed the experiments. D.C. performed the aptamer selection and validation. Z.W. performed the chip fabrication and wrote the code for AptaZ. All authors discussed the results, analysed the data and contributed to the preparation and editing of the manuscript.

Competing interests

S.O.K. is an inventor on a patent entitled 'Device for capture of particles in a flow' (US patent US10073079) that is licensed to CTRL Therapeutics. The remaining authors declare no competing interests.

Additional information

Supplementary information The online version contains supplementary material available at https://doi.org/10.1038/s41557-023-01207-z.

Correspondence and requests for materials should be addressed to Shana O. Kelley.

Peer review information *Nature Chemistry* thanks Chunhai Fan, Yingfu Li and the other, anonymous, reviewer(s) for their contribution to the peer review of this work.

nature research

Corresponding author(s): Shana Kelley

Last updated by author(s): Apr 1, 2023

Reporting Summary

Nature Research wishes to improve the reproducibility of the work that we publish. This form provides structure for consistency and transparency in reporting. For further information on Nature Research policies, see our Editorial Policies and the Editorial Policy Checklist.

Statistics

For all statistical analyses, confirm that the following items are present in the figure legend, table legend, main text, or Methods section.

n/a	Confirmed
☐	☒ The exact sample size (*n*) for each experimental group/condition, given as a discrete number and unit of measurement
☐	☒ A statement on whether measurements were taken from distinct samples or whether the same sample was measured repeatedly
☒	☐ The statistical test(s) used AND whether they are one- or two-sided *Only common tests should be described solely by name; describe more complex techniques in the Methods section.*
☒	☐ A description of all covariates tested
☒	☐ A description of any assumptions or corrections, such as tests of normality and adjustment for multiple comparisons
☐	☒ A full description of the statistical parameters including central tendency (e.g. means) or other basic estimates (e.g. regression coefficient) AND variation (e.g. standard deviation) or associated estimates of uncertainty (e.g. confidence intervals)
☒	☐ For null hypothesis testing, the test statistic (e.g. *F*, *t*, *r*) with confidence intervals, effect sizes, degrees of freedom and *P* value noted *Give P values as exact values whenever suitable.*
☒	☐ For Bayesian analysis, information on the choice of priors and Markov chain Monte Carlo settings
☒	☐ For hierarchical and complex designs, identification of the appropriate level for tests and full reporting of outcomes
☒	☐ Estimates of effect sizes (e.g. Cohen's *d*, Pearson's *r*), indicating how they were calculated

Our web collection on statistics for biologists contains articles on many of the points above.

Software and code

Policy information about availability of computer code

Data collection	Flow cytometry data were collected using Cytoflex flow cytometer and its software, CytExpert(version 2.4).
Data analysis	FlowJo (Version 10.5.3) for flow cytometry data analysis. Prism GraphPad (version 8.0.1) for data plot and statistic analysis. Raw deep sequencing data were processed using using USEARCH (v10) and Cutadapt (V3.5). M-fold for DNA strucrture analysis.

For manuscripts utilizing custom algorithms or software that are central to the research but not yet described in published literature, software must be made available to editors and reviewers. We strongly encourage code deposition in a community repository (e.g. GitHub). See the Nature Research guidelines for submitting code & software for further information.

Data

Policy information about availability of data

All manuscripts must include a data availability statement. This statement should provide the following information, where applicable:

- Accession codes, unique identifiers, or web links for publicly available datasets
- A list of figures that have associated raw data
- A description of any restrictions on data availability

The main data supporting the results in this study are available within the paper and its supplementary information. The source data underlying Figs. 1d, e, 2c, d, h, i, j, 3b, c, e, f, g, 4b, c, and Supplementary Figs 4, 5, 6, 10, 11, 12 are provided as a Source Data file.The sequencing data files are too large to be publicly shared, but they are available from the corresponding author upon reasonable request. The chip design (in the format of STL) and running protocol of the microfluidic chip will be available free of charge from the publisher's website as a supplementary file.

Field-specific reporting

Please select the one below that is the best fit for your research. If you are not sure, read the appropriate sections before making your selection.

☒ Life sciences ☐ Behavioural & social sciences ☐ Ecological, evolutionary & environmental sciences

For a reference copy of the document with all sections, see nature.com/documents/nr-reporting-summary-flat.pdf

Life sciences study design

All studies must disclose on these points even when the disclosure is negative.

Sample size	For most cases, triplicate measurement were performed unless otherwise noted. Details on sample size for experiments were indicated in Methods and figure legends. No statistical methods were used to predetermine the sample size. Sample size for experiments was estimated based on previous experience with similar setups that showed significance. Triplicate measurement is gold standard for the characterization of aptamer binding interactions and allows the determination of of sample-to-sample variance.
Data exclusions	No data was excluded.
Replication	Experiments were performed with three replication and the findings were successfully reproduced.
Randomization	Each sample was tested under the same experimental conditions. The in-vitro tests were conducted in a well-controlled environment so no randomization was required.
Blinding	No blinding was required as the identity of each sample was known prior to each measurement.

Reporting for specific materials, systems and methods

We require information from authors about some types of materials, experimental systems and methods used in many studies. Here, indicate whether each material, system or method listed is relevant to your study. If you are not sure if a list item applies to your research, read the appropriate section before selecting a response.

Materials & experimental systems

n/a	Involved in the study
☐	☒ Antibodies
☒	☐ Eukaryotic cell lines
☒	☐ Palaeontology and archaeology
☒	☐ Animals and other organisms
☒	☐ Human research participants
☒	☐ Clinical data
☒	☐ Dual use research of concern

Methods

n/a	Involved in the study
☒	☐ ChIP-seq
☐	☒ Flow cytometry
☒	☐ MRI-based neuroimaging

Antibodies

Antibodies used	Anti-biotin microbeads ultrapure (#130-105-637)
Validation	The antibody was validated by the manufacturer and has been referenced by at least 32 publications.

Flow Cytometry

Plots

Confirm that:

☒ The axis labels state the marker and fluorochrome used (e.g. CD4-FITC).

☒ The axis scales are clearly visible. Include numbers along axes only for bottom left plot of group (a 'group' is an analysis of identical markers).

☒ All plots are contour plots with outliers or pseudocolor plots.

☒ A numerical value for number of cells or percentage (with statistics) is provided.

Methodology

Sample preparation	No cells or biological samples are used. Aptamer particles were prepared as outlined in the methods section. The partiucles were incubated with the target before staining.
Instrument	Cytoflex (Beckman Coulter)
Software	FlowJo software (FlowJo LLC)
Cell population abundance	This is not relevant because no cells were used in the flow cytometry experiments.
Gating strategy	Particles were first gated by FSC/SSC followed by duplicates discrimination SSC-H/SSC-A. See Figure S3a.

☒ Tick this box to confirm that a figure exemplifying the gating strategy is provided in the Supplementary Information.